JOURNAL OF THERMOPHYSICS AND HEAT TRANSFER
Vol. 6, No. 3, July–Sept. 1992

Thermochemical Nonequilibrium Flow Computations of Flow Around the Aeroassist Flight Experiment

Grant Palmer*
NASA Ames Research Center, Moffett Field, California 94035

A three-dimensional explicit, finite rate, shock-capturing, numerical algorithm is used to calculate thermochemical nonequilibrium flowfields about the Aeroassist Flight Experiment (AFE) vehicle at one of its flight trajectory points. The governing equations are expressed in cylindrical coordinates to alleviate perturbations in solution along the three-dimensional grid singular line. The full Navier-Stokes equations and an 11-species chemical model with the latest reaction rates are incorporated into the code. Pressure, heat transfer, and temperature data are presented.

Nomenclature

c_s	=	mass fraction of species s
D	=	binary diffusion coefficient
e	=	total energy per unit volume
e_v	=	vibrational energy per unit volume
$\hat{e}_v$	=	vibrational energy per unit mass
$\boldsymbol{E}, \boldsymbol{F}, \boldsymbol{G}, \boldsymbol{H}$	=	inviscid flux vectors
g_0, g_1, g_2	=	degeneracy factors
h_s^o	=	heat of formation of species s
K_{eq}	=	equilibrium constant
k	=	Boltzmann's constant, 1.3805×10^{-16} erg/K
k_f, k_b	=	forward and backward rate constants
M	=	molar mass
N_A	=	Avogadro's number, 6.0225×10^{23}
p	=	pressure
$\boldsymbol{Q}$	=	vector of conservative variables
q, q_v	=	heat conduction
R	=	universal gas constant
Re	=	Reynolds number, $\rho_\infty c_\infty l/\mu_\infty$
$\boldsymbol{R}, \boldsymbol{S}, \boldsymbol{T}, \boldsymbol{U}$	=	viscous flux vectors
T	=	translational temperature
T_v	=	vibrational temperature
t	=	time
u, v, w	=	flow velocities in x, y, z directions
$u_s, v_{rs}, u_{\theta s}$	=	diffusion velocities in x, r, θ directions
$\boldsymbol{W}$	=	source term vector
$\dot{w}$	=	chemical source term
X_s	=	mole fraction
x, r, θ	=	cylindrical coordinate directions
x, y, z	=	Cartesian coordinate directions
β	=	real-gas equation of state parameter
θ_d	=	characteristic temperature of dissociation
θ_{vs}	=	charactistic temperature of vibration
θ_1, θ_2	=	characteristic temperature of electronic excitation
κ	=	thermal conductivity
κ_v	=	vibrational thermal conductivity
μ	=	viscosity
ξ, η, ζ	=	generalized coordinate directions
ρ	=	density
Σ_m	=	summation of molecular species quantity

Presented as Paper 90-1702 at the AIAA/ASME 5th Joint Thermophysics and Heat Transfer Conference, Seattle, WA, June 18–20, 1990; received July 25, 1990; revision received Nov. 15, 1990; accepted for publication Aug. 1, 1991.

*Research Scientist, Aerothermodynamics Branch. Member AIAA.

Introduction

THE Aeroassist Flight Experiment (AFE) vehicle, a major element of NASA's Civilian Space Technology Initiative, is scheduled for launch in 1996. Released from the Space Shuttle, the AFE will pass through the earth's atmosphere and be recovered by the Shuttle. Its primary purposes are to demonstrate the viability of aerobraking as a means of planetary entry, and to gather experimental data that will be used to validate real-gas computational fluid dynamic codes.

The AFE will travel in the Earth's upper atmosphere at velocities ranging from 7 to 10 km/s. At these conditions, both chemical and thermal nonequilibrium effects will be significant. It is impossible to duplicate this flow regime in ground-based test facilities. Newly developed real-gas Navier-Stokes codes are being used along with older boundary-layer and viscous shock-layer techniques to approximate the aerodynamic and thermal loads the AFE will experience, and to design the experiments carried aboard the spacecraft.

The three-dimensional shock-capturing, fully coupled, thermochemical nonequilibrium algorithm presented in this work uses a two-temperature physical model to account for thermal nonequilibrium effects and finite rate chemical reactions to describe the dissociation and ionization in the high-temperature region behind the bow shock. The code solves the full Navier-Stokes equations and utilizes new vibrational relaxation time parameters for determining the Landau-Teller vibrational relaxation time. Thirty finite rate chemical reactions are used to determine the chemical composition of an 11-species air mixture. The code has been vectorized reducing the time to compute one iteration at one point from 1.95×10^{-4} s for an unvectorized 7-species model[1] to 9.5×10^{-5} s for the current 11-species code.

Numerical solutions generated with the code have been compared with experimental and computational data in an attempt to validate the method.[1] Additional comparisons against recent three-dimensional AFE flow calculations are included in this study. Surface pressure distributions are compared against other numerical techniques, and convective heating rates on the forebody calculated by the present code are compared with those produced using boundary-layer and viscous shock-layer techniques.

Governing Equations

The three-dimensional Navier-Stokes equations, including species continuity equations, represent the conservation of mass, momentum, and energy. They are usually expressed in Cartesian coordinates. This presents a problem when flow is computed over a blunt, rounded vehicle such as the AFE. The grid normally used for this type of problem consists of a series of radial planes that meet at a singular line. Along this

singular line, the metric terms used in the generalized transformation are either zero or indeterminate and must, therefore, be extrapolated in some manner from the interior. This approximate determination of the metric terms leads to nonphysical oscillations and perturbations in the flow solution near the singular line.

One way to alleviate this difficulty is to express the governing equations in cylindrical rather than Cartesian coordinates. The system is then transformed into a generalized *cylindrical* coordinate system. The metric terms can then be evaluated directly with no approximation involved. As before, the Navier Stokes equations consist of conservation equations for species mass, global mass, momentum, total energy, and vibrational energy, except now the three components of momentum per unit volume are $[\rho u, \rho v_r, \rho u_\theta]$ where v_r and u_θ are the velocity components in the r and θ directions. In vector form, the equations are

$$\frac{\partial \boldsymbol{Q}}{\partial t} + \frac{\partial \boldsymbol{E}}{\partial x} + \frac{\partial \boldsymbol{F}}{\partial r} + \frac{1}{r}\frac{\partial \boldsymbol{G}}{\partial \theta} + \frac{\boldsymbol{H}}{r} = \frac{\partial \boldsymbol{R}}{\partial x} + \frac{\partial \boldsymbol{S}}{\partial r} + \frac{1}{r}\frac{\partial \boldsymbol{T}}{\partial \theta} + \frac{\boldsymbol{U}}{r} + \boldsymbol{W} \tag{1}$$

where

$$\boldsymbol{Q} = \begin{bmatrix} \rho_1 \\ \vdots \\ \rho_s \\ \rho \\ \rho u \\ \rho v_r \\ \rho u_\theta \\ e \\ e_v \end{bmatrix} \quad \boldsymbol{E} = \begin{bmatrix} \rho_1(u + u_1) \\ \vdots \\ \rho_s(u + u_s) \\ \rho u \\ \rho u^2 + p \\ \rho u v_r \\ \rho u u_\theta \\ (e + p)u \\ e_v u + \Sigma_s e_{vs} u_s \end{bmatrix}$$

$$\boldsymbol{F} = \begin{bmatrix} \rho_1(v_r + v_{r1}) \\ \vdots \\ \rho_s(v_r + v_{rs}) \\ \rho v_r \\ \rho u v_r \\ \rho v_r^2 + p \\ \rho v_r u_\theta \\ (e + p)v_r \\ e_v v_r + \Sigma_s e_{vs} v_{rs} \end{bmatrix} \quad \boldsymbol{G} = \begin{bmatrix} \rho_1(u_\theta + u_{\theta 1} \\ \vdots \\ \rho_s(u_\theta + u_{\theta s}) \\ \rho u_\theta \\ \rho u u_\theta \\ \rho v_r u_\theta \\ \rho u_\theta^2 + p \\ (e + p)u_\theta \\ e_v u_\theta + \Sigma_s e_{vs} u_{\theta s} \end{bmatrix}$$

$$\boldsymbol{H} = \begin{bmatrix} \rho_1(v_r + v_{r1}) \\ \vdots \\ \rho_s(v_r + v_{rs}) \\ \rho v_r \\ \rho u v_r \\ \rho v_r^2 - \rho u_\theta^2 \\ 2\rho v_r u_\theta \\ (e + p)v_r \\ e_v v_r \end{bmatrix} \quad \boldsymbol{R} = \begin{bmatrix} 0 \\ \vdots \\ 0 \\ 0 \\ \tau_{xx} \\ \tau_{xr} \\ \tau_{x\theta} \\ q_x + q_{vx} + u_j\tau_{xj} - \Sigma_s \rho_s u_s h_s \\ q_{vs} \end{bmatrix}$$

$$\boldsymbol{S} = \begin{bmatrix} 0 \\ \vdots \\ 0 \\ 0 \\ \tau_{xr} \\ \tau_{rr} \\ \tau_{r\theta} \\ q_r + q_{vr} + u_j\tau_{rj} - \Sigma_s \rho_s v_{rs} h_s \\ q_{vr} \end{bmatrix}$$

$$\boldsymbol{T} = \begin{bmatrix} 0 \\ \vdots \\ 0 \\ 0 \\ \tau_{x\theta} \\ \tau_{r\theta} \\ \tau_{\theta\theta} \\ q_\theta + q_{v\theta} + u_j\tau_{\theta j} - \Sigma_s \rho_s u_{\theta s} h_s \\ q_{v\theta} \end{bmatrix}$$

$$\boldsymbol{U} = \begin{bmatrix} 0 \\ \vdots \\ 0 \\ 0 \\ \tau_{xr} \\ \tau_{rr} - \tau_{\theta\theta} \\ 2\tau_{r\theta} \\ q_r + q_{vr} + u_j\tau_{rj} - \Sigma_s \rho_s v_{rs} h_s \\ q_{vr} \end{bmatrix}$$

$$\boldsymbol{W} = \begin{bmatrix} \bar{w}_1 \\ \vdots \\ \bar{w}_s \\ 0 \\ 0 \\ 0 \\ 0 \\ 0 \\ \Sigma_m(Q_{T-V_s} + \bar{w}_s \bar{e}_{vs}) - p_e \dfrac{\partial u_j}{\partial x_j} - \Sigma_{\text{ions}} \dot{n}_{e,f} E_{i,f} \end{bmatrix}$$

where

$$u_j\tau_{xj} = u\tau_{xx} + v_r\tau_{xr} + u_\theta\tau_{x\theta}$$

$$q_x = \kappa \frac{\partial T}{\partial x}$$

$$q_{vr} = \kappa_v \frac{\partial T_v}{\partial r}$$

and so on. The shear stresses are given by

$$\tau_{xx} = \frac{2}{3}\mu\left[2\frac{\partial u}{\partial x} - \frac{\partial v_r}{\partial r} - \frac{1}{r}\frac{\partial u_\theta}{\partial \theta} - \frac{v_r}{r}\right]$$

$$\tau_{rr} = \frac{2}{3}\mu\left[2\frac{\partial v_r}{\partial r} - \frac{\partial u_x}{\partial x} - \frac{1}{r}\frac{\partial u_\theta}{\partial \theta} - \frac{v_r}{r}\right]$$

$$\tau_{\theta\theta} = \frac{2}{3}\mu\left[\frac{2}{r}\frac{\partial u_\theta}{\partial \theta} - \frac{\partial v_r}{\partial r} - \frac{\partial u}{\partial x} + 2\frac{v_r}{r}\right]$$

$$\tau_{xr} = \mu\left[\frac{\partial u}{\partial r} + \frac{\partial v_r}{\partial x}\right]$$

$$\tau_{x,\theta} = \mu\left[\frac{1}{r}\frac{\partial u}{\partial \theta} + \frac{\partial u_\theta}{\partial x}\right]$$

$$\tau_{r\theta} = \mu\left[\frac{1}{r}\frac{\partial v_r}{\partial \theta} + r\frac{\partial (u_\theta/r)}{\partial r}\right]$$

The cylindrical grid coordinates and velocities can be converted back to the Cartesian frame by the relations

$$y = r\cos\theta \quad z = r\sin\theta$$

$$v = \cos\theta v_r - \sin\theta u_\theta \quad w = \sin\theta v_r + \cos\theta u_\theta \tag{2}$$

The system is transformed in a generalized coordinate system. The Jacobian and metric terms of this new system are

$$J = [x_\xi(r_\eta\theta_\zeta - r_\zeta\theta_\eta) - x_\eta(r_\xi\theta_\zeta - r_\zeta\theta_\xi) + x_\zeta(r_\xi\theta_\eta - r_\eta\theta_\xi)]^{-1}$$

$$\xi_x = J(r_\eta\theta_\zeta - \theta_\eta r_\zeta)$$

$$\xi_r = J(x_\zeta\theta_\eta - \theta_\zeta x_\eta)$$

$$\xi_\theta = J(r_\zeta x_\eta - x_\zeta r_\eta)$$

$$\eta_x = J(r_\zeta\theta_\xi - \theta_\zeta r_\xi)$$

$$\eta_r = J(x_\xi\theta_\zeta - \theta_\xi x_\zeta)$$

$$\eta_\theta = J(x_\zeta r_\xi - x_\xi r_\zeta)$$

$$\zeta_x = J(r_\xi\theta_\eta - \theta_\xi r_\eta)$$

$$\zeta_r = J(x_\eta\theta_\xi - \theta_\eta x_\xi)$$

$$\zeta_\theta = J(r_\eta x_\xi - x_\eta r_\xi) \tag{3}$$

A general gas in thermal nonequilibrium is characterized by a translational, rotational, and electron temperature as well as a vibrational temperature for each diatomic and polyatomic species present. To simplify this model, the translational and rotational temperatures are assumed to equilibrate quickly. Further, it is assumed that one vibrational temperature characterizes the vibrational state of all diatomic and polyatomic species, and the electron temperature is equal to this vibrational temperature. This two-temperature model[2] consists of one translational and one vibrational temperature. Two energy equations, total and a combined vibrational-electronic, must be solved.

An equation can be written relating the total energy and translational temperature

$$e = 1.5\bar{R}T\sum_{s\neq e}\frac{\rho_s}{M_s} + \bar{R}T\sum_{m}\frac{\rho_s}{M_s} + e_v + e_{el} + \tfrac{1}{2}\rho(u^2 + v_r + u_\theta) + \sum_s \rho_s h_s^o \tag{4}$$

The first two terms are the energy of translation and rotation. The vibrational temperature can be obtained from

$$e_v = \sum_m \frac{\rho_s\bar{R}}{M_s}\frac{\theta_{vs}}{e^{\theta_{vs}/T_v} - 1} + 1.5\frac{\rho_e}{M_e}\bar{R}T_v \tag{5}$$

The first term in Eq. (5) relates the vibrational energy to the vibrational temperature by the equation of a harmonic oscillator. In the two-temperature model, the translational energy of the electron is characterized by the vibrational temperature and this term is included in the equation for the vibrational-electronic energy. A Boltzmann distribution of electronic states characterized by the vibrational temperature T_v is assumed. The energy of electronic excitation, significant only for some of the species present, is given by the expression

$$e_{el} = \sum_{n,o,o_2,n^+,o^+,n_2^+}\frac{\rho_s\bar{R}}{M_s}\left[\frac{\theta_1 g_1 e^{-\theta_1/T_v} + \theta_2 g_2 e^{-\theta_2/T_v}}{g_0 + g_1 e^{-\theta_1/T_v} + g_2 e^{-\theta_2/T_v}}\right] \tag{6}$$

The quantities e, e_v, ρ, and ρ_s used in Eqs. (4–6) are obtained from the solution of the conservation equations. The pressure can be related to the other global conservation quantities by the relation

$$p = \sum_{s\neq e}\frac{\rho_s}{M_s}\bar{R}T + \frac{\rho_e}{M_e}\bar{R}T_v \tag{7}$$

Energy Exchange Mechanism and Heat Conduction

The rate of energy exchange between the vibrational and translational modes is taken from Park[2]

$$Q_{T-V_s} = \frac{e_{vs}^*(T) - e_{vs}}{\tau_{vs}}\left|\frac{T_{shk} - T_v}{T_{shk} - T_{v\ shk}}\right|^{S_s - 1} \tag{8}$$

This is a modified form of the Landau-Teller formulation. The quantity $e_{vs}^*(T)$ is the vibrational energy evaluated using the translational temperature. The postshock translational and vibrational temperatures are T_{shk} and $T_{v\ shkj}$. The postshock vibrational temperature is taken to be the freestream temperature.[3] The relaxation time τ_{vs} is the sum of the Landau-Teller relaxation time and a collision-limited relaxation time that corrects for the fact that the Landau-Teller relaxation rate is unrealistically high at high temperatures.[2] The quantity within the absolute value bracket in Eq. (8) in an empirical bridging function that accounts for the diffusive nature of the energy exchange that occurs at high vibrational temperatures. Equation (8) was derived to match experimentally observed conditions behind a normal shock wave. Its validity in regions of expansion has not been confirmed.

Transport Properties

Calculating multicomponent diffusion is a complicated and computationally intensive process. As a simplification, the binary diffusion model was used in this study. A further simplification is to assume a constant binary diffusion coefficient for each species pair. This is acceptable if the constituents of the gas are of similar molecular weight and have similar collision integral values and collision diameters. The diffusion mass flux of species s can be expressed by[4]

$$\rho_s u_{sj} = -\rho\frac{1 - c_s}{1 - X_s}D\frac{\partial c_s}{\partial x_j} \tag{9}$$

The method for determining the viscosity and thermal conductivity of the 11-species gas mixture is taken from Gupta et al.[5]

Chemical Model

The 30 chemical reactions used in this study were taken from Park.[6] Eleven species, N, N_2, O, O_2, NO, N^+, O^+, N_2^+, O_2^+, NO^+, and e^-, were considered. For a sample reaction

$$AB + M \rightleftharpoons A + B + M$$

The change in the amount of constituent AB in moles per cubic meter is

$$\frac{d[AB]}{dt} = -k_f[AB][M] + k_b[A][B][M] \tag{10}$$

The forward and backward reaction rates are of the form

$$k_f(T) = C_f T^{\eta_f} e^{-\theta_d/T} \quad k_b(T) = \frac{k_f(T)}{K_{eq}(T)} \tag{11}$$

The reaction rate constants in Eq. (11) were obtained from Park.[6] For heavy-particle impact dissociation reactions, the forward rate is dependent on the vibrational excitation of the diatomic molecule and the kinetic energy of the impacting particle. The temperature that governs the forward reaction rate is taken to be the geometric average of the translational and vibrational temperatures[2] $\sqrt{TT_v}$. The reverse reaction is dependent upon the relative velocities of the impacting particles and is governed only by the translational temperature.

For exchange reactions among neutral species, the forward and backward rates are assumed to be governed only by the relative velocities of the impacting particles and, hence, only

on the translational temperature. The forward rate of association ionization reactions will also depend only upon the translational temperatures, but the reverse rate will depend upon the vibrational temperatures and the translational temperature of the electron, both of which are equal to the vibrational temperature T_v in the two-temperature model.

The equilibrium constants $K_{eq}(T)$ were found using the equation[7]

$$K_{eq}(T) = \exp(A_1 + A_2 z + A_3 z^2 + A_4 z^3 + A_5 z^4) \quad (12)$$

where

$$z = 10{,}000/T$$

For dissociative recombination, associative ionization, and electron-impact ionization reactions, the equilibrium constant K_{eq} is evaluated in the two-temperature model using the vibrational temperature.

Solution Algorithm

The presence of strong flow gradients such as shocks requires the use of some form of upwind differencing to maintain stability during the flow computation. The differencing used in the present algorithm is Van Leer flux-vector splitting.[8] The solutions presented in this paper were computed using first-order spatial differencing of the inviscid fluxes. However, the inclusion of second-order differencing is a relatively simple procedure using the transition operators developed in Ref. 9.

The numerical solutions were all impulsively started; that is, initially the flow was freestream everwhere. Freestream values were maintained along the supersonic inflow boundary. The outflow boundary was also assumed to be supersonic, and zero-order extrapolation from the interior was used. The no-slip condition and zero normal pressure gradient were imposed on the wall. The wall was assumed to be noncatalytic. The AFE solutions all utilized a fixed temperature wall boundary condition.

The governing equations are solved using an explicit formulation. Normally, the inclusion of species continuity equations with source terms derived from finite rate chemical reactions renders an explicit algorithm stiff, meaning that prohibitively small time-steps are required to maintain stability. However, in previous studies[1,9] a technique was developed that overcomes this stiffness problem. Essentially, it scales the species mass fraction updates obtained after each iteration so the largest change in any species mass fraction is no larger than a certain prescribed value. The method has successfully computed flows over a wide range of freestream conditions and has been corroborated with comparisons to both experimental data and computations using other explicit and implicit techniques.

Results

In a previous study, numerical results from the explicit two-temperature code were compared against an extensive set of experimental and computational data for the purposes of code validation.[1] These comparisons demonstrated the accuracy and validity of the algorithm. Flow was computed over the AFE vehicle at a trajectory point altitude of 77.8 km where the AFE is traveling at 8914 m/s. A 85 × 23 × 85 grid constructed in three patches was used for the computation. A constant temperature of 1650 K was imposed on the AFE forebody as a wall boundary condition. This temperature was chosen to compare results against previous computations. The temperature on the back of the AFE was held fixed to 750 K. In the skirt region, the wall temperature was blended from 750 to 1650 K.

The effect of using the cylindrical formulation can be seen in a plot of velocity contours near the forebody singular line of the AFE grid. The forebody singular and stagnation line are nearly coincident. Figure 1a is the solution using the Cartesian formulation. A nonphysical perturbation of the contours in the singular line region is clearly evident, mainly due to the fact that the v and w components of velocity do not approach zero near the singular/stagnation line as they should. Figure 1b shows velocity contours using the same grid when the cylindrical formulation is employed. The velocity contours are now smooth and continuous near the singular line because the computed v_r and u_θ components of velocity do approach zero near the singular/stagnation line.

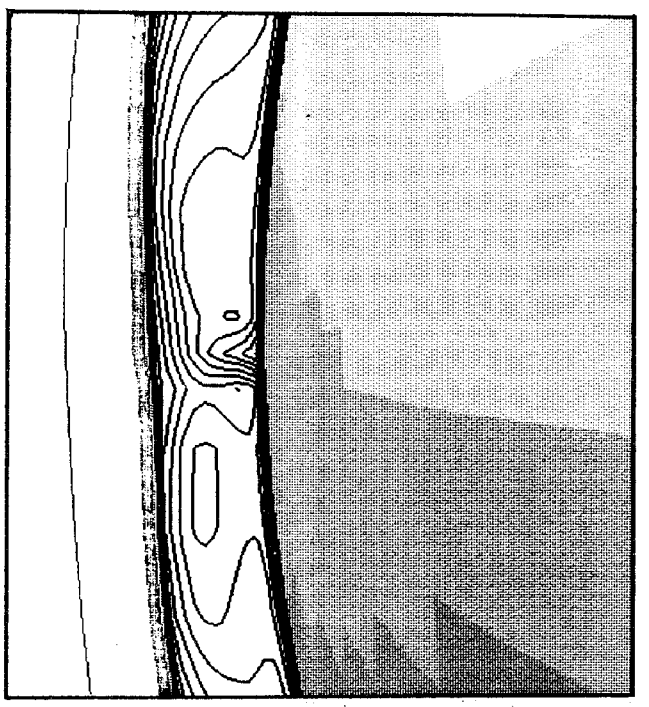

Fig. 1a Velocity contours, Cartesian formulation.

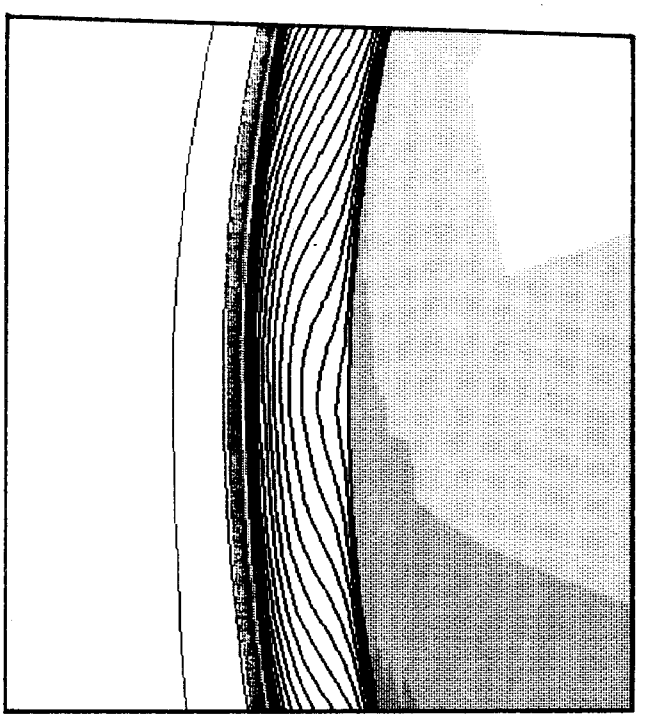

Fig. 1b Velocity contours, cylindrical formulation.

Figures 2a and 2b show stagnation line translational and vibrational temperature profiles. Compared to the present results are those from Gnoffo[10] using a point-implicit method, a Direct-Simulatoin Monte Carlo (DSMC) solution from Moss,[11] and the shock-fitting, three-dimensional flow solution of Tam.[12] These represent four fundamentally direct algorithms for computing nonequilibrium flows.

The translational temperature profiles and bow shock locations are very similar for three of the codes, Tam's solution shows a flatter profile that rises to a higher peak at a larger shock standoff distance. Tam also predicts a lower vibrational temperature than the other solutions. These differences might be attributed to the fact that Tam's code was the only one to employ a shock-fitting rather than a shock-capturing technique. Shock-fitting assumes the shock wave is infinitestimally thin, a questionable assumption at 77.8 km altitude.

The present study shows a different vibrational temperature profile shape, but it is believed this can be attributed to two things. Gnoffo, Moss, and Tam all used the reaction rate set of Kang et al.[13] Their results all show the peak vibrational temperature along the stagnation line very close to the shock. The nonequilibrium flow computations of Candler,[3] who used Park's reaction rates, show a peak vibrational temperature

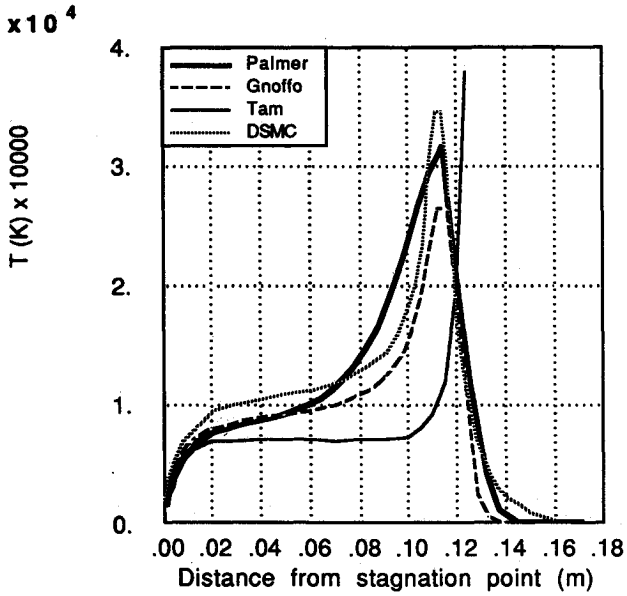

Fig. 2a Stagnation line translational temperature profile.

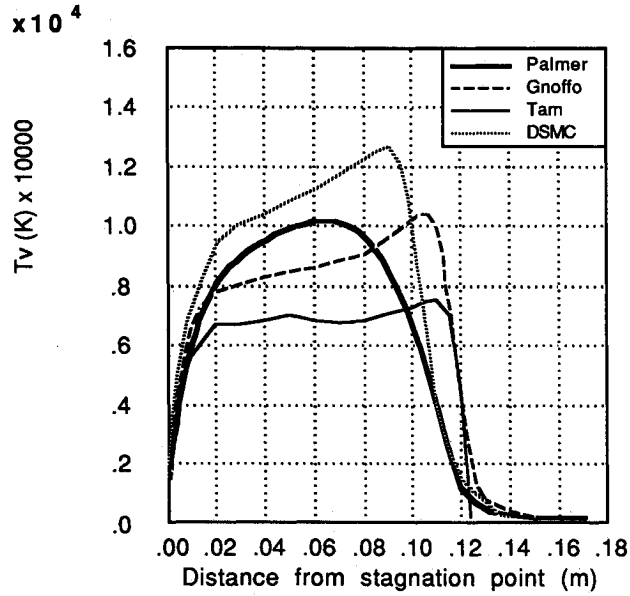

Fig. 2b Stagnation line vibrational temperature profile.

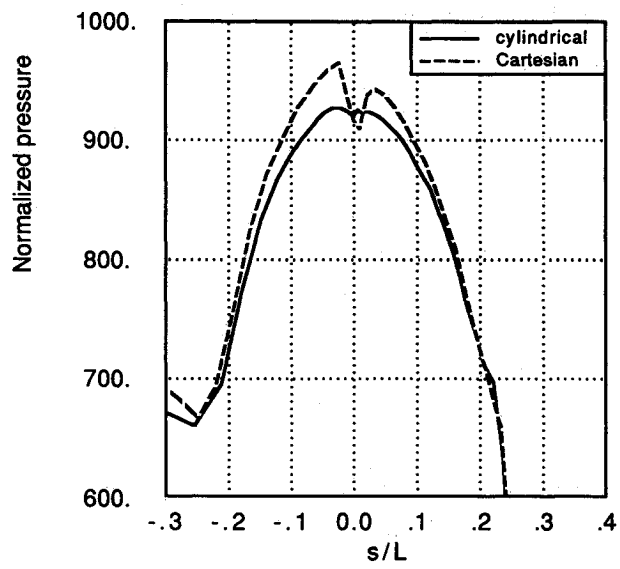

Fig. 3 Surface pressure along pitch-plane.

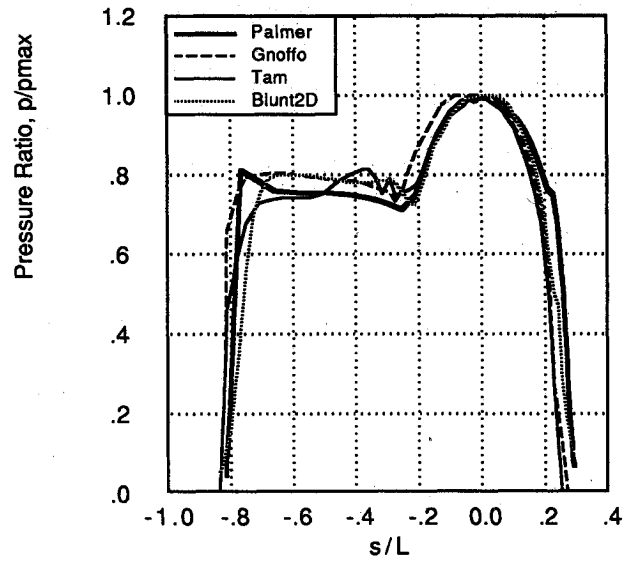

Fig. 4 Surface pressure ratio along pitch-plane.

further behind the shock, similar to that shown by the present work, at altitudes above 70 km. Gnoffo, Moss, and Tam also did not include the empirical bridging function in their expression for the translational-vibrational energy exchange mechanism. This would give their solutions a greater energy exchange from the translational to the vibrational modes than that shown in this work.

The next series of plots show surface quantities along the forebody pitch plane. Figure 3 shows forebody surface pressure normalized by $\rho_\infty c_\infty^2$ along the pitch-plane. The quantity s/L is the normalized distance along the pitch-plane with $s/L = 0$ being the stagnation point, $s/L = 0.282$ the shoulder of the short side, and $s/L = 0.82$ the shoulder of the long side. This plot again illustrates the improvement in the solution quality when the cylindrical formulation is used. The Cartesian solution exhibits a discontinuity in the value of computed surface pressure near the singular line. This discontinuity affects the pressure profile along virtually the entire forebody. The cylindrical solution shows a nearly continuous pressure profile throught the singular line.

Figure 4 compares the surface pressure ratio, p/p_{max}, along the pitch-plane. Shown are the predictions of the present work, Gnoffo, Tam, and those from the Blunt2D computer code.[14] Blunt2D is an inviscid, axisymmetric, equilibrium code. All four codes produced very similar surface pressure distri-

butions on the short side of the pitch-plane. Gnoffo's solution indicates a higher pressure ratio on the long side than the other methods. The fact that an axisymmetric inviscid equilibrium code predicted virtually the same surface pressure as the three-dimensional viscous, thermochemical, nonequilibrium codes indicates that computing pressure distributions is not a sufficient test of the accuracy or validity of a method because the AFE at 77.8 km is in a region where viscous and nonequilibrium effects are important.

One of the most difficult challenges thermochemical, nonequilibrium, Navier-Stokes codes face is the accurate prediction of surface heat transfer. Older methods, such as boundary-layer and viscous shock-layer techniques, generally give more accurate heat transfer values. An attempt was made to compare heat transfer calculated by the present code to that computed by the Boundary Layer Integral Matrix Procedure (BLIMP88) code[14] corrected by stagnation point viscous shock-layer results.

Figure 5 shows convective heating on the AFE pitch-plane as a function of distance from the stagnation point. The BLIMP88 profile consists of a flat dome that extends over

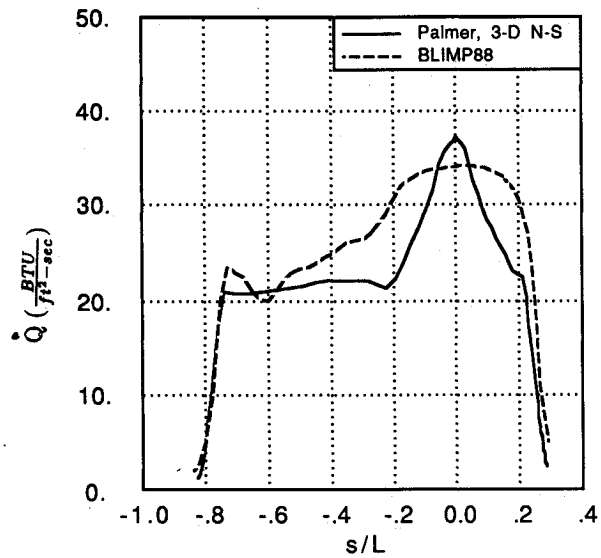

Fig. 5 Convective heat transfer along pitch-plane.

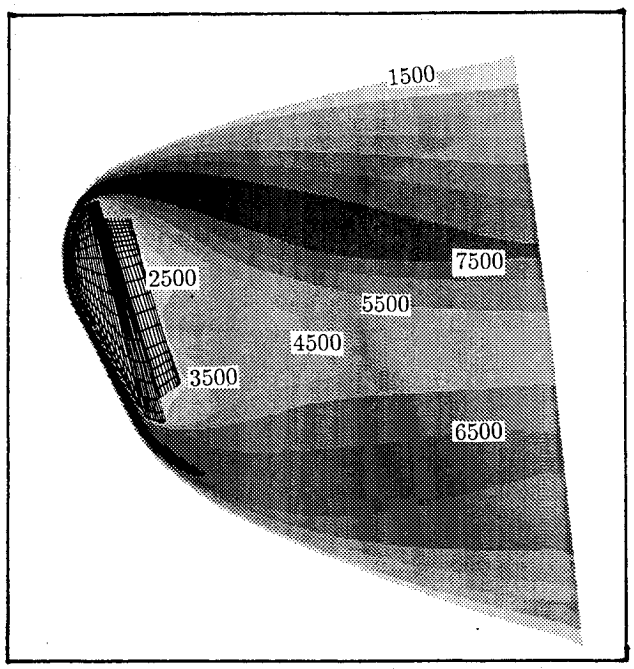

Fig. 6 Vibrational temperature contours (K).

most of the circular nose region. The heating rate then declines rapidly on the short side. On the long side, the heating rate declines more gradually with a local peak as the flow reaches the edge of the forebody.

The Navier-Stokes heating prediction showed a higher stagnation point value of convective heating. The rate then fell off quite sharply to the edge of the circular nose region. The profile-flattened out on the long side and failed to pick up much of the local peak. The shape of the profile along the circular nose region was found to be strongly grid-dependent. The original grid did not have adequate clustering to resolve the temperature gradients properly. With further reduction of the minimum spacing near the wall, the stagnation line value of convective heating became higher and the peak near the stagnation point broader. Further grid refinement is probably necessary for optimum heating prediction. The heating profile from $s/L = -0.2$ to $s/L = -0.8$, the flat part of the long side, shows a nearly constant heating rate that was not grid-dependent. The level of heating in this region remained fairly constant during the various grid refinements.

One of the experiments to be carried aboard the AFE will measure the radiation in the baseflow region of the vehicle. To design and calibrate the instruments, it is necessary to know the approximate level of radiation expected in the base region. One of the necessary quantities to compute radiation is the vibrational temperature. Figure 6 shows computed vibrational temperature contours around the AFE. Higher values of vibrational temperature are shown as darker contours. The peak vibrational temperature of 11,200 K occurs along the forebody stagnation line. As the flow expands around the shoulder of the vehicle, the chemical composition and vibrational temperature effectively freeze. The vibrational temperature remains relatively high over a large portion of the base region. The darkest contour band extending backward from the shoulder on the short side corresponds to vibrational temperatures of 7500–8000 K.

There is some question as to whether first-order differencing is acceptable for the base region computation. Important phenomena, such as a recirculating core, are apparent in the present solution. Far more grid points were used in the base region in this calculation than were used in Refs. 10 and 12 compensating somewhat for the use of first-order differencing. Questions such as whether the two-temperature model is applicable for expanding flows and, if it is not, what physical model should be used, are larger in magnitude than those presented by using first-order differencing of the inviscid fluxes.

A three-dimensional, AFE flowfield solution using the code and grid presented in this study requires about 15,000 iterations. This corresponds to 65 h of CPU time on a Cray-2 supercomputer. The code's efficiency is approximately 9.5×10^{-5} s/point/iteration.

Conclusion

The explicit code described in this study was simplistic in its formulation and has demonstrated its ability to compute flows accurately in thermochemical nonequilibrium. It was found that using a cylindrical formulation of the grid and governing equations substantially reduces nonphysical solution perturbations caused by the three-dimensional, singular line.

Flow was computed over the AFE vehicle at its 77.8 km flight trajectory point. Three different nonequilibrium Navier-Stokes codes predicted similar translational temperature profiles and shock standoff distances along the stagnation line of the AFE. The differences seen in the vibrational temperature profiles may be related to the reaction rate set and energy exchange mechanisms used.

Although predicting surface pressure is not a conclusive test, accurately computing surface heat transfer is a difficult challenge for three-dimensional, thermochemical nonequilibrium Navier-Stokes codes. It was found that the calculated heat transfer rate was very grid-dependent. Some of this might

be alleviated by using second-order differencing for the inviscid fluxes, but it seems to be important to cluster grid lines tightly near the body surface, especially near the stagnation region. The heat transfer predicted by the Navier-Stokes code presented in this work compared reasonable well with that predicted by the boundary-layer code BLIMP88. Further grid refinement is necessary to optimize the Navier-Stokes calculation.

There is still much work to be done on the AFE problem. Resolving the physics and grid sensitivity of the flow in the base region of the AFE and refining the surface convective heating rate calculation will be the focus of future studies.

References

[1]Palmer, G., "The Development of an Explicit Thermochemical Nonequilibrium Algorithm and Its Application to Compute Three Dimensional AFE Flowfields," AIAA Paper 89-1701, Buffalo, NY, 1989.

[2]Park, C., "Assessment of Two-Temperature Kinematic Model for Ionizing Air," AIAA Paper 87-1574, Honolulu, HI, 1987.

[3]Candler, G., "The Computation of Weakly Ionized Hypersonic Flows in Thermochemical Nonequilibrium," Ph.D. Thesis, Stanford Univ., Stanford, CA, 1988.

[4]Hirschfelder, J. O., Curtiss, C. F., and Bird, R. B., *Molecular Theory of Gases and Liquids*, Wiley, New York, 1954.

[5]Gupta, R., Yos, J., and Thompson, R., "A Review of Reaction Rates and Thermodynamic and Transport Properties for the 11-Species Air Model for Chemical and Thermal Nonequilibrium Calculations to 30000K," NASA TN 101528, 1989.

[6]Park, C., "A Review of Reaction Rates in High Temperature Air," AIAA Paper 89-1740, Buffalo, NY, 1989.

[7]Park, C., "On Convergence of Computation of Chemically Reacting Flows," AIAA Paper 85-0247, Reno, NV, 1985.

[8]Anderson, W. K., Thomas, J. L., and Van Leer, B., "Comparison of Finite Volume Flux Vector Splittings for the Euler Equations," *AIAA Journal*, Vol. 24, No. 9, 1986, pp. 1453–1460.

[9]Palmer, G. E., "An Improved Flux-Split Algorithm Applied to Hypersonic Flows in Chemical Equilibrium," AIAA Paper 88-2693, San Antonio, TX, 1988.

[10]Gnoffo, P. A., Gupta, R. N., and Shinn, J. L., "Conservation Equations and Physical Models for Hypersonic Air Flows in Thermal and Chemical Nonequilibrium," NASA TP 2867, 1989.

[11]Moss, J. N., Bird, G. A., and Virendra, K. D., "Nonequilibrium Thermal Radiation for an Aeroassist Flight Experiment Vehicle," AIAA Paper 88-0081, Reno, NV, 1988.

[12]Tam, L., and Li, C., "Three-Dimensional Thermal and Chemical Nonequilibrium Flow Modeling for Aeroassist Flight Experiment," AIAA Paper 89-1860, Buffalo, NY, 1989.

[13]Kang, S. W., Jones, W. L., and Dunn, M. G., "Theoretical and Measured Electron-Density Distributions at High Altitudes," *AIAA Journal*, Vol. 11, No. 2, 1973, p. 141–149.

[14]Ting, P. C., Rochelle, W. C., Mueller, S. R., Colovin, J. E., Scott, C. D., and Curry, D. M., "Development of AFE Aerobrake Aerothermodynamic Data Book," AIAA Paper 89-1734, Buffalo, NY, 1989.